LIGHTWEIGHT STRUCTURES in CIVIL ENGINEERING
CONTEMPORARY PROBLEMS
Monograph from Scientific Seminar
Organized by Polish Chapters of
International Association for Shell and Spatial Structures
Lodz University of Technology
Faculty of Civil Engineering, Architecture and Environmental Engineering
XXIV LSCE
Łódź, 7th of December 2018 (Friday)

DYNAMIC RESPONSE OF A TENSEGRITY SIMPLEX IN IMPACT HAMMER TESTS

L. Małyszko[1)], A. Rutkiewicz[2)], P. Bilko[3)]
[1)] Associate professor, *leszek.malyszko@uwm.edu.pl*,
[2)] Assistant, *andrzej.rutkiewicz@uwm.edu.pl*, [3)] *PhD,* Assistant, *piotr.bilko@uwm.edu.pl,*
Faculty of Geodesy, Geospatial and Civil Engineering, University in Olsztyn, POLAND

ABSTRACT: The paper presents the modal parameters investigation of the simplex tensegrity prism (unit with three compressed bars and nine tensioned cables). An emphasis is put on the pre-stress level influence on the natural frequencies and vibration modes (two different levels are analysed). The form-finding procedure and the force density relations in elements are developed theoretically. A physical model of the prism is described and investigated experimentally using impact testing hammer and three-axial accelerometers. The recorded data for each pre-stress level is composed of nine setups, in which one impulse signal and nine acceleration signals are analysed. The results show first five natural frequencies, vibration modes and damping ratios, although only first two natural frequencies clearly rise with the increased prestress level. In addition, it is shown that recording only one second of acceleration and impulse signals is sufficient to gather all the needed information which can be further utilized for the structural health monitoring purposes.

Keywords: modal parameters extraction, impact hammer test, tensegrity simplex, pre-stress level

1. INTRODUCTION

Tensegrity systems are composed of compressed bars and elastic tensioned cables connected in nodes in such a way that stability of the system under external loads applied at the nodes can only be achieved by the pre-stress of the cables. This pre-stress state often called the self-stress state is an initial internal equilibrium state and to a high degree determines the stiffness and stability to the structure. Since the members of tensegrity structures are commonly seen as pin-jointed elements, they can be regarded as a special class of spatial truss structures where the members are assembled in a self-equilibrated system. The well-known example of such a structure is the Snelson's tower - a column composed of several units attached to each other – so called the simplex units (Ref.1) (Fig. 1). The three bars simplex with triangular bases shown in Fig. 1b is a fundamental three-dimensional unit often called a regular minimal tensegrity *T3* prism, (Ref.2). It contains three bars that connect vertices of the two equilateral horizontal triangles. The top and bottom triangles are formed by three cables. The remaining three cables also connect the vertices of the top triangle to the vertices of the bottom triangle. The unit is constructed as a spatial truss of twelve members from three compressed bars and nine tensioned cables. If the upper triangle is rotated counter-clockwise with respect to the bottom triangle by an angle of 5/6π about the vertical axis of the simplex it is then often called a left-handed. When the *T3* unit is right-handed the upper triangle is rotated clockwise by the same angle (Figs 1b, 2).

Tensegrities structures can experience large displacements and hence their analysis should include geometrical nonlinearity with response to loading dependent on the pre-stress level. A comprehensive survey on simplex static response to axial loading was done in the range of numerical analysis in (Ref 3). The numerical study, which was further proved by experiments in (Ref.4), showed that the simplex prisms may present extreme stiffening-type response or extreme softening response, which is a matter of aspect ratio of the structure, the magnitude of the applied prestress and material properties of the members. Based on nonlinear static analyses some design examples of the simplex units with cables made of innovative materials were also presented in (Refs. 5,6) together with an incremental iterative procedure given a Matlab code. However, after a designed pre-

Fig. 1 a) the Snelson's sculpture (Ref. 1), b) the left-handed simplex (top) and the right-handed simplex (bottom)

stressing is introduced by a lengthening or shortening of some members from their unstrained lengths, the response can often be linearized, as is the common case in simulation approaches. Having a non-linear static equilibrium state for a chosen internal pre-stress level, the small vibrations of the structure around the considered equilibrium can be analyzed with its modal characteristics, natural frequencies and related eigenvectors. Identified modal characteristics can be used for the calibration and validation of dynamic structural models. The first natural frequency in tensegrity structures is very important. It marks the stiffness of the structure and is most susceptible to changes, when this stiffness changes – due to the pre-stress decrease, cross-string slack or bar buckling. That is why it is utilized in vibrational health monitoring or structural control.

One of the first static and dynamic test of a tensegrity simplex was performed by (Ref.7) in 1987, where a response to axial loading and forces in elements were studied, while dynamic behaviour in terms of first six eigenfrequencies were obtained below the level of 100Hz. In (Ref.8) a numerical investigation on the pre-stress influence on the eigenfrequencies of tensegrity 2D structures was studied. It was shown that for a certain tensegrity structure, increasing the level of pre-stress may cause the eigenfrequencies to rise or fall. S. Amouri (Ref.9) studied a dynamic response of a actuator controlled tensegrity model created in the Tensarch project (Ref.10). The authors developed a control strategy for attenuating first vibration modes in the studied category of structures. A compressive study on a five module tensegrity structure was given in (Ref.11) – the numerical and experimental results on dynamic behaviour and, additionally, vibration control by small movements of active struts. The influence of the pre-stress on the axial stiffness and response of the simplex, as well as some other tensegrity models, was recently investigated numerically in (Ref.12), where also a usability of the tensegrity concept in road bridges was studied.

This paper presents the modal parameters of the simplex unit that were obtained through an experimental study on an own physical model. Recorded data in impact hammer tests was matched with one of the system identification methods and afterwards modal parameters were extracted using an appropriate Matlab toolbox for experimental and operational modal analysis (Ref.13). The paper is organized as follows: section 2 consists of the mathematical explanation of self-stress states in the analysed simplex prism, section 3 includes experimental modal analysis with deep explanation of the construction of the physical model and finally, section 4 is enclosing the paper with results and conclusions.

2. REFERENCE CONFIGURATION AND PRE-STRESS STATE

The equilibrium equations of the right-handed simplex can be written for the top nodes P_4, P_5 and P_6 in a linearized vector form as (Fig. 2)

$$\begin{cases} \mathbf{N}_{41}+\mathbf{N}_{43}+\mathbf{N}_{45}+\mathbf{N}_{46}=\mathbf{F}_4 \\ \mathbf{N}_{51}+\mathbf{N}_{52}+\mathbf{N}_{54}+\mathbf{N}_{56}=\mathbf{F}_5 \\ \mathbf{N}_{62}+\mathbf{N}_{63}+\mathbf{N}_{64}+\mathbf{N}_{65}=\mathbf{F}_6 \end{cases}, \tag{1}$$

where the vectors $\mathbf{F}_i$ denote the external nodal forces in the *i*-node.

The number of a non-trivial solution to the equilibrium Eqn (1) when $\mathbf{F}=\mathbf{0}$ indicates the number of the self-stress states. It also represents the number of pre-stressing devices which are needed to establish the compatible self-stress state in the tensegrity structure that ensures tension in cables and compression in bars.

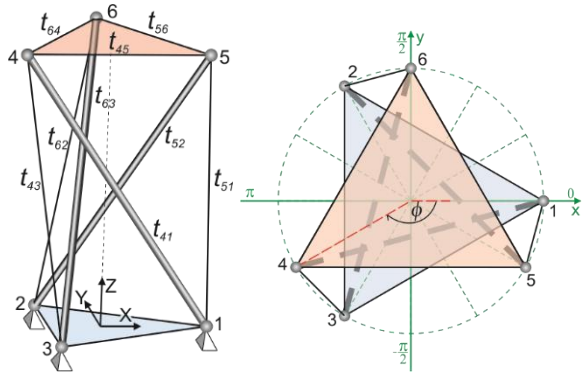

Fig. 2 The right-handed simplex with notations and a coordinate system

The force vector of the arbitrary member P_i-P_k in Eqn (1) can be calculated as $\mathbf{N}_{ki}=N_{ki}P_kP_i$, where N_{ki} is a scalar of force magnitude and P_kP_i is a versor calculated as $P_kP_i=\overrightarrow{P_kP_i}/L_{ki}$, where L_{ki} is the member length equal to norm of the $\overrightarrow{P_kP_i}$ vector. Introducing force densities as $t_{ki}=N_{ki}/L_{ki}$ the vector $\mathbf{N}_{ki}$ is $\mathbf{N}_{ki}=N_{ki}/L_{ki}\cdot\overrightarrow{P_kP_i}$, where the vector $\overrightarrow{P_kP_i}$ contains the components in terms of nodes coordinates $\{(X_i-X_k),\ (Y_i-Y_k),\ (Z_i-Z_k)\}$ of the initial node P_k and the end node P_i in the Cartesian coordinate system $\{\mathrm{X},\mathrm{Y},\mathrm{Z}\}$.

In the coordinate system, which has the origin at the center of mass of the bottom base triangle, the coordinates of the nodes $P_i\{X_i\ \ Y_i\ \ Z_i\}$ are identified as

$$\begin{aligned} &P_1\{r\ \ 0\ \ 0\},\quad P_2\{-r/2\ \ r\sqrt{3}/2\ \ 0\},\quad P_3\{-r/2\ \ -r\sqrt{3}/2\ \ 0\},\\ &P_4\{r\cos\varphi\ \ r\sin\varphi\ \ h\},\quad P\{r\cos(\varphi+2\pi/3)\ \ r\sin(\varphi\ \ 2\pi/3)\ \ h\},\\ &P_6\{r\cos(\varphi+4\pi/3)\ \ r\sin(\varphi+4\pi/3)\ \ h\}, \end{aligned} \tag{2}$$

where the radius is $r=L/\sqrt{3}$.

Three variables L, φ and h can describe the initial geometry of the unit with a vertical axis and two horizontal equilateral triangles. The height h denotes the distance separating the two horizontal triangles, L is the side length of the equilateral triangles. The horizontal triangles can be rotated with the respect to each other by the angle of twist φ.

Based on the Eqn (1) with the vector of the force densities (Fig. 2)

$$\begin{pmatrix} \frac{\sqrt{3}}{3}\cos(\phi)+\frac{1}{2} & -2\frac{\sqrt{3}}{3}\sin^2\left(\frac{\phi}{2}\right) & \cos\left(\frac{\pi}{6}-\phi\right) & 0 & 0 & 0 & 0 & 0 & \cos\left(\phi+\frac{\pi}{6}\right) \\ \frac{\sqrt{3}}{3}\sin(\phi)+\frac{1}{2} & \frac{\sqrt{3}}{3}\sin(\phi) & -\sin\left(\frac{\pi}{6}-\phi\right) & 0 & 0 & 0 & 0 & 0 & \sin\left(\phi+\frac{\pi}{6}\right) \\ \frac{h}{L} & \frac{h}{L} & 0 & 0 & 0 & 0 & 0 & 0 & 0 \\ 0 & 0 & -\sin(\phi) & -\frac{\sqrt{3}}{3}\sin\left(\phi+\frac{\pi}{6}\right)-\frac{\sqrt{3}}{3} & -2\frac{\sqrt{3}}{3}\cos\left(\frac{\phi}{2}+\frac{\pi}{6}\right)\sin\left(\frac{\phi}{2}\right) & -\cos\left(\frac{\pi}{6}-\phi\right) & 0 & 0 & 0 \\ 0 & 0 & \cos(\phi) & \frac{\sqrt{3}}{3}\cos\left(\phi+\frac{\pi}{6}\right) & -2\frac{\sqrt{3}}{3}\sin\left(\frac{\phi}{2}+\frac{\pi}{6}\right)\sin\left(\frac{\phi}{2}\right) & \sin\left(\frac{\pi}{6}-\phi\right) & 0 & 0 & 0 \\ 0 & 0 & 0 & \frac{h}{L} & \frac{h}{L} & 0 & 0 & 0 & 0 \\ 0 & 0 & 0 & 0 & 0 & \sin(\phi) & 2\frac{\sqrt{3}}{3}\cos\left(\frac{\pi}{6}-\frac{\phi}{2}\right)\sin\left(\frac{\phi}{2}\right) & 2\frac{\sqrt{}}{3}\cos\left(\frac{\pi}{6}-\frac{\phi}{2}\right)\sin\left(\frac{\phi}{2}\right) & -\cos\left(\ +\frac{\pi}{6}\right) \\ 0 & 0 & 0 & 0 & 0 & -\cos(\phi) & -2\frac{\sqrt{3}}{3}\cos\left(\frac{\pi}{6}-\frac{\phi}{2}\right)\cos\left(\frac{\phi}{2}\right) & -2\frac{\sqrt{3}}{3}\sin\left(\frac{\pi}{6}-\frac{\phi}{2}\right)\sin\left(\frac{\phi}{2}\right) & -\sin\left(\phi+\frac{\pi}{6}\right) \\ 0 & 0 & 0 & 0 & 0 & 0 & \frac{h}{L} & \frac{h}{L} & 0 \end{pmatrix} \tag{4}$$

$$\{t_{43}, t_{41}, t_{45}, t_{51}, t_{52}, t_{46}, t_{62}, t_{63}, t_{56}\} \quad (3)$$

the equilibrium matrix on the left side of Eqn (1) has the form presented in Eqn (4) along with a row numbering scheme to be equivalent to ordering of the measurement displacements

$$\{u_{4X}, u_{4Y}, u_{4Z}, u_{5X}, u_{5Y}, u_{5Z}, u_{6X}, u_{6Y}, u_{6Z}\}. \quad (5)$$

Hence, the simplex unit is treated as the structure of the nine degrees of freedom, i.e. nine displacements of the top nodes.
The square equilibrium matrix (4) is rank-deficient for $\varphi = -5\pi/6$. The null-space of the matrix gives the one state of self-stress, **ns**, in terms of an arbitrary constant, the force density t:

$$\mathbf{ns} = \{t\sqrt{3}, -t\sqrt{3},\ t,\ t\sqrt{3}, -t\sqrt{3},\ t,\ t\sqrt{3}, -t\sqrt{3},\ t\}. \quad (6)$$

As one can see from (6), it is reasonable to assume the following self-stress state for the unloaded unit without the supports:

$$\begin{aligned} &t_{43} = t_{51} = t_{62} = t\sqrt{3} \\ &t_{45} = t_{46} = t_{56} = t_{12} = t_{13} = t_{23} = t\ . \\ &t_{41} = t_{52} = t_{63} = -t\sqrt{3} \end{aligned} \quad (7)$$

The detailed initial geometry of the simplex unit used in the tests is given in Tab.1 together with the assumed self-stress.

Table 1. Geometry of the simplex unit used in the tests ($\varphi = -5\pi/6$)

Self-stress state									
t_{41} (bars)			t_{45} (base cables)			t_{43} (cross cables)			
-1			$1/\sqrt{3}$			1			
L_{41} [m]			L_{45} [m]			L_{43} [m]			
0.9378			0.4872			0.7781			
Node	Coordinates [m]			Node and member numbers					
	X	Y	Z						
1	0.281	0	0	Base cables				Cross cables	
2	-0.141	0.243	0	1	1-2	4	4-5	10	1-5
3	-0.141	-0.243	0	2	2-3	5	5-6	11	2-6
4	-0.243	-0.141	0.764	3	3-4	6	4-6	12	3-4
5	0.243	-0.141	0.764	Bars					
6	0	0.281	0.764	7	1-4	8	2-5	9	3-6

It is worth noting that three unknown force densities are needed if during the deformation of the simplex unit the top and bottom triangles remain parallel to each other. This may happen if the unit is under uniform axial loading.

3. VIBRATION EXPERIMENTS

3.1. Small free vibrations of the tensegrity structure

The small free vibrations of the tensegrity structure around the non-linear equilibrium state with the chosen pre-stress level can be obtained from a linearized eigenproblem

$$\mathbf{K}_T \boldsymbol{\varphi}_k - \omega_k^2 \mathbf{M} \boldsymbol{\varphi}_k = \mathbf{0}, \quad (8)$$

where $\mathbf{K}_T$ is the tangent stiffness matrix and $\mathbf{M}$ is the mass matrix of the structure.
The spectral decomposition of the matrix $\mathbf{M}^{-1}\mathbf{K}_T$ yields the natural frequencies and corresponding mode shapes of the tensegrity structure. For the considered equilibrium state with *(n)* active degrees of freedom the spectral decomposition of the generalized eigenproblem (8) gives *(n)* the frequencies ω_k $(\omega_1 < \omega_2 ... < \omega_n)$ and the related eigenvectors $\boldsymbol{\varphi}_k$.
The matrices $\mathbf{K}_T$ and $\mathbf{M}$ are usually assembled for the structure from the element matrices $\mathbf{k}_T$ and $\mathbf{m}$ given in the local coordinates according to the known algorithm of the Finite Element Method. The tangent element stiffness matrix $\mathbf{k}_T$ is decomposed into an element elastic stiffness $\mathbf{k}_E$ and a geometric stiffness matric $\mathbf{k}_G$ according to

$$\mathbf{k}_T = \mathbf{k}_E + \mathbf{k}_G, \quad (9)$$

where the matrix $\mathbf{k}_G$ is dependent on the pre-stress level.
In general, the elastic and geometric stiffness matrices are evaluated while the structure is in equilibrium expressed by displacement coordinates for all nodes. This equilibrium should be obtained iteratively due to geometric nonlinearity, also for the pre-stress level without external loads.
It is worth noting that the axial response can only be found with the truss formulation without bending moments which can appear during transversal vibrations. The transversal modes of vibration can be the most visible modes during an environmental excitation. The chosen finite element must be able to capture the bending behavior with a stiffness affected by the current axial force, even if the bending stiffness of tensioned members is low and affects the structure response to a very low degree.

3.2. Pre-stress setting of the experimental model

The experiments described in this paper were conducted on the full-scale simplex specially made for this study. The model with mounted three piezoelectric sensors on its top is shown in Fig. 3. It is made of three steel bars of 20 [mm] the nominal diameter with the yield and failure strengths of 640 and 800 [MPa], respectively. The circular bars

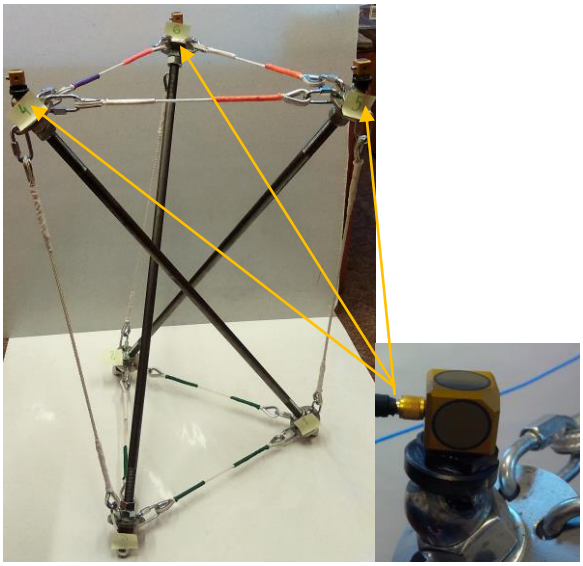

Fig. 3 The simplex model with three sensors on the top nodes

have been threaded to the M20 nominal thread on the length of 150 [mm] on both ends providing connection points to move in order to execute the pre-stress. Two types of polyamide lines are used for the cables: a writhed, three strand line with 6 [mm] diameter for the cross cables and a braided line with core and a diameter of 4 [mm] for the others. The failure parameters of the lines are presented in Tab. 2 as stated by the manufacturer. Each bar gets through the centre of the node plate with three openings. The opening are made for snap hooks enabling to mount the lines with thimbles. The plate is 6 [mm] thick and made of AISI 304 (EN 1.4301) stainless steel.

Table 2. Failure parameters of the lines provided by the manufacturer

Failure load (6 mm) [N]	Failure strain (6 mm) [%]	Failure load (4 mm) [N]	Failure strain (4 mm) [N]
7400	43	3100	unspecified

The mechanical parameters of the lines had to be checked before the assembly to the model because the lines were plaited into the thimble in different ways (supposed local weakening of the material) and had different types of rope strand. It is important to emphasise, that the stranded rope has different mechanical properties than the material from which it is tangled (that is why the Youngs modulus of the lines made with different tangles is different that the Youngs modulus of the polyamide material itself). The tension tests of the plaited lines were conducted on a universal testing machine of 10 [kN] nominal force. Eight specimens, four of each diameter were tested with a speed of 10 [mm/min] up to the failure (Fig. 4). The Young's modulus for the cross cables was calculated as a secant between the two points corresponding to the strain values between 2 and 4 [%], as the cables in the pre-stress stages were working in that range and, consequently, the modulus for the base cables was calculated as a secant between 0.6 and 1.2 [%]. The results are presented in Tab. 3 and in Fig. 5.

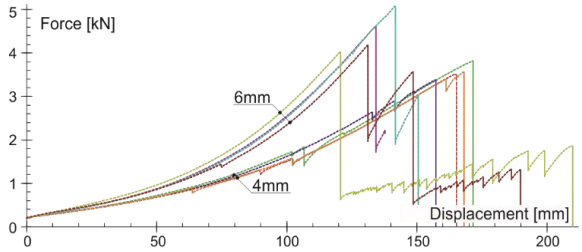

Fig. 4 The Force-displacement diagrams of polyamide lines

Table 3. Polyamide lines parameters after plaiting into the thimble

Failure load [N]	Tension strength [MPa]	Failure strain [%]	Youngs modulus [MPa]
6 mm diameter			
4478.7±469.9	158.4±16.6	43.8±3	121.4±17.7
4 mm diameter			
3568.3±180.7	284±14.4	34.1±1.2	327.8±15.5

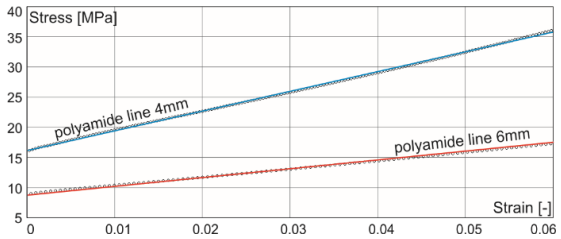

Fig. 5 The Stress-strain diagram of polyamide lines failure tests

The pre-stressing means the introducing of internal forces in the externally unloaded tensegrity structure and can be defined in different ways. It is often introduced by a lengthening or shortening of some members from their unstrained lengths. This method of pre-stressing is implemented here based on the analytical model presented in (Ref.5). To describe the self-stress state the pre-stress level p_0 is introduced which is defined as a normal elongation of the cross cables, i.e. as the strain

$$p_0 = \frac{s_0 - s_N}{s_N} \tag{9}$$

where s_0 is the reference length of the cross cable after the initial pre-strain and s_N is its natural or rest length.

It follows from (9) that the length of the cross cable is $s_0 = s_N(1+p_0)$ after introducing the pre-stress state of the level p_0. The other reference lengths, the side length of the horizontal triangles L_0 and the bar length b_0, as well as the related normal forces in the bars, cross-cables and base cables can be calculated based on the analytical model form (Ref.5). These lengths can also be achieved iteratively while using the finite element method or they can be measured in situ. This last rough method of in situ measurements is used here in a preliminary analysis together with the calculated lengths from the analytical model. Rotations of the M20 nuts on each bar thread enable the pre-stressing by changing the distances between the bar ends. The change of the bar lengths causes the lengthening of the cables without changing the twist angle φ.

Three pre-stress levels are discussed here (Tab. 4). The first level of pre-stress (indexed 0 in Tab. 4) is assumed to be very close to the natural state, as the aim was to create as little internal forces as possible. However, the knowledge of the exact natural state is unknown. Assuming that one full rotation of the M20 nuts equals 2.5 [mm] of the change of the bar length, the other two levels (indexed 1 and 4) are known from the increase of the bar lengths in the following manner: level 1 – the length increase of 15 [mm] (six rotations) and level 4 – the length increase of 30 [mm] (twelve rotations) – each rotations counting from the level 0.

The differences between the calculated and measured dimensions are not greater than 0,8 [%] for the cross strings and 0,5 [%] for the base strings, which is an acceptable value due to the accuracy of in situ measurement techniques and node solutions.

Table 4. Lengths of the simplex members [m]

No	p_0 [%]	Bars	Base cables	Cross cables	Height	*Measured lengths
0	0	0.9378	0.4872	0.7781	0.7643	
1	2.05	0.9528	0.4902	0.7940	0.7804	
			0.4914*		0.7845*	
4	4.10	0.9687	0.4931	0.8099	0.7964	
			0.4972*		0.7995*	

3.3. Vibration measurements

Among three types of dynamic vibration tests: forced, ambient and combined, the forced vibration testing with the impact hammer was used here. This test method yields good results for relatively small mechanical devices tested in laboratory condition. It is assumed in this test that all forces that are applied to the structure are measured while ambient forces like wind or traffic loads can be excluded. However, the basis of an experimental determination of the vibration properties in dynamic vibration tests is a properly and accurately measured signal of accelerations, generally from few transducers, and an excitation force in the time domain. At the excitation, transducers send an analogous electrical signal in a form of a continuous function as an input. The signal is amplified by the amplifier. Next, the analyzer performs a digitization of the analogous signal into discrete series with utilization of the anti-aliasing filter. The time resolution (number of samples measured in time) is dependent on the sampling rate, while the resolution of the recorded magnitudes is dependent on the bit depth.

A complete measuring system is usually composed of three elements: an excitation mechanism, a power amplifier, an analyzer and at least one transducer. The presented survey was conducted on the equipment available in the Institute of Building Engineering - the analyzer with dedicated software, the transducer and the blow hammer. The amplifier and the analyzer are often placed in a single device, as is the case of the utilized analyzer. The tests were performed using a data acquisition and recording system TEAC brand, model LX-110 (Fig. 6).

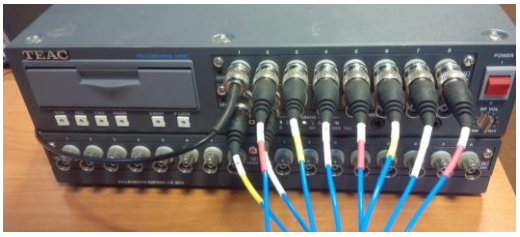

Fig. 6. The acquisition and recording unit

It is a unit able to record voltage, sound, vibration and strains at a bandwidth of 40 [kHz]. The unit operates 32 channels simultaneously with the maximum number of 128 channels). Basic technical data is presented in Tab. 5.

Table 5. Basic technical data of the unit

Sampling frequency [kHz]	Available Voltage [V]	Maximum speed of recording [MB/s]	Bandwidth [Bit]
1.5/3/6/12/24/48/96	±0.5/1/2/5/10/20/50	1.6	16/24

The received electrical signal is amplified to the level visible by the analyzer. The process of measuring is controlled by dedicated software. The purpose of piezoelectric transducers is to generate electrical impulses due to the occurrence of a mechanical shock. The transducers used in the experiment are the typical triaxial accelerometers consisting of a seismic mass and piezoelectric crystals enclosed in a one body. Manufacturer parameters of sensor are gathered in Tab. 6.

Table 6. The PCB 356B18 transducer parameters

Type of transducer	accelerometer	Resonant frequency	≥10 [kHz]
Sensitivity (±5%)	102 [mV/(m/s^2)]	Non-linearity	≤ 1 [%]
Measurement range	±49 [m/s^2 pk]	Transverse sensitivity	≤ 7 [%]
Frequency range (±5%)	0.5 to 2000 [Hz]	Self-weight	225 [g]
Frequency range (±10%)	0.3 to 4000 [Hz]	Screwing momentum	3-7 [Nm]

The impact hammer generates the impulse load and serves as an excitation mechanism in the test. The hammer is composed of a handle integrated with a striking head, which is a sensor working analogously to the accelerometer, although giving information on the force values. An additional mass and a set of hammer tips enables to adjust the stiffness of the hammer surface and its mass in order to induce the desired frequency component of the structure. The general rule is that the smaller the weight of the hammer and the greater the rigidity of the tip, the higher frequencies are excited. Characteristics of the hammer are gathered in Tab. 7.

Table 7. The 086C03 impulse hammer parameters

Sensitivity (±15%)	2.25 [mV/N]	Non-linearity	≤ 1 [%]
Range	±2224 [N pk]	Hammer mass	160 [g]
Resonance frequency	≥22 [kHz]	Extender mass weight	73.7 [g]

Three tri-axial acceleration sensors were mounted on each node of the upper triangle of the simplex structure, on the nodes no 4, 5 and 6 (Fig.3). The sensors mass equals 25 [gm] and is insignificant with the mass of the 20 [mm] diameter steel bars. Fixing the bottom triangle during measurements to the floor, the simplex can be treated as the structure of nine degrees of freedom, three DOFs for each upper node. In accordance to the global coordinate system in Fig. 2, it was possible to measure in one setup accelerations of nine signals 4x, 4y, 4z, 5x, 5y, 5z, 6x, 6y, 6z together with one force signal from the impulse hammer as a source of excitation. After a preliminary broadband test of determining the natural frequencies and modes shapes of the simplex, nine separate setups of detailed modal identification tests were carried out for each prestress level with excitation of different node and direction (Tab. 8).

Table 8. Setups and applied impulse force for each pre-stress level

Setup	1	2	3	4	5	6	7	8	9
Excitation	4x	4y	4z	5x	5y	5z	6x	6y	6z

In general, the modal analysis consists of (1) data collecting with processing gathered signals, (2) system identification and (3) modal characteristics estimation. The last step of extracting and validating a set of modal parameters can be determined from a free vibration analysis of the identified system model. The identified system model is a mathematical model estimated from measured data and can be parametric or nonparametric, in which case the system is described in tabulated form, for instance as numerical Frequency Response Function (FRF) data. The modal parameters can be determined from a modal decomposition of the identified system model. All these three steps of the modal analysis presented in the article are developed using the Macec program (Ref.13). It is a Matlab (Ref.14) toolbox that enables among others two classical experimental modal analysis approaches: the nonparametric FRF estimation and the deterministic poly-reference least squares complex frequency domain method (pLSCF). The second was utilized in the test and is characterized with a very clear stabilization diagrams given with small computational effort. The detailed information on the computational algorithm exceeds the volume of the article – for more guidance please refer to Refs 15-16.

3.4. Signals processing and modal parameters

The signals were recorded with a relatively high, for the test purposes, sampling frequency of 1500 [Hz]. The sampling frequency was chose to be as high to capture the short-time transient signals of the impact in full detail. On the other hand it is the lowest setup option for the possessed recorder. Each signal lasted approximately 15 seconds. The further processing of signals included the removal of the offset and the decimation by 10. This process enabled to obtain the maximum value of frequency equal to 75 [Hz] in accordance to the Nyquist frequency and aliasing phenomena. The summary of the modal characteristics based on the all recorded signals are shown in Tab. 9 for the pre-stress level one and four. Some other results are presented in figures below.

Table 9. Predicted variation of natural frequencies [Hz] and damping ratios [%]

Mode	1	2	3	4	5
Pre-stress level 1					
f [Hz]	3.32	8.84	28.61	48.21	60.19
ξ [%]	1.7	3.1	2.5	0.7	1.3
Pre-stress level 4					
f [Hz]	4.12	9.67	30.85	47.14	60.04
ξ [%]	1.1	2.3	1.5	0.4	1.4

Figures 7 and 8 presents the results of the setup 1, for which the impulse is applied to the node 4 and in the direction X. From the nine signals recorded in this setup the signal 4x in the direction X is only presented here for the pre-stress level 1 (Fig. 7) and 4 (Fig 8). These signals are extracted from the direction X of the accelerometer in the node 4.

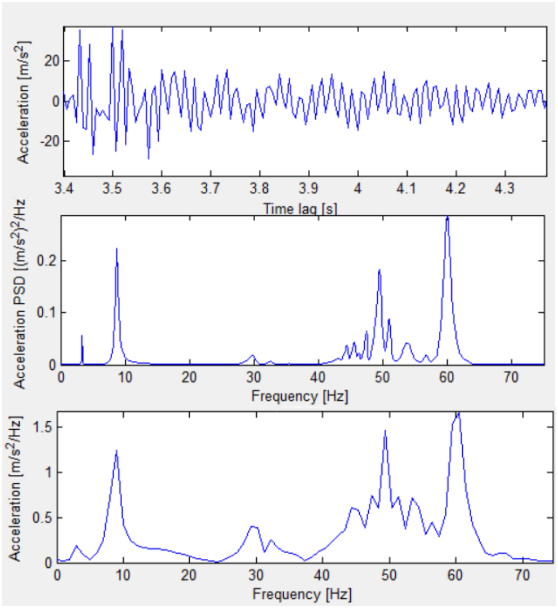

Fig. 7 Setup 1, pre-stress level 1, signal 4x: (from top to bottom) square acceleration in time domain, power spectral density (PSD) of the acceleration and the acceleration in frequency domain

The increased pre-stress level, which is related to the increased stiffness of the simplex unit, caused the values of acceleration to rise as seen in Fig. 7 and 8 on the vertical axes. The first natural period of vibrations has decreased significantly after the pre-stressing of the simplex to the level four (Tab. 9). As one can see in the diagrams of the acceleration and the acceleration PSD of the first pre-stress level, a concentration of natural frequencies seems to occur around the value of 50 [Hz]. After the pre-stressing, the modes are more clearer and sharper, as if the dominant frequency would be excited, and the nearing ones were not. The tendency of increasing the natural frequencies is visible in the acceleration plot mainly for the first three modes, although it is not of great significance. This is due to the fact, that the stiffness of the cables are very small in relation to the stiffness of the bars.

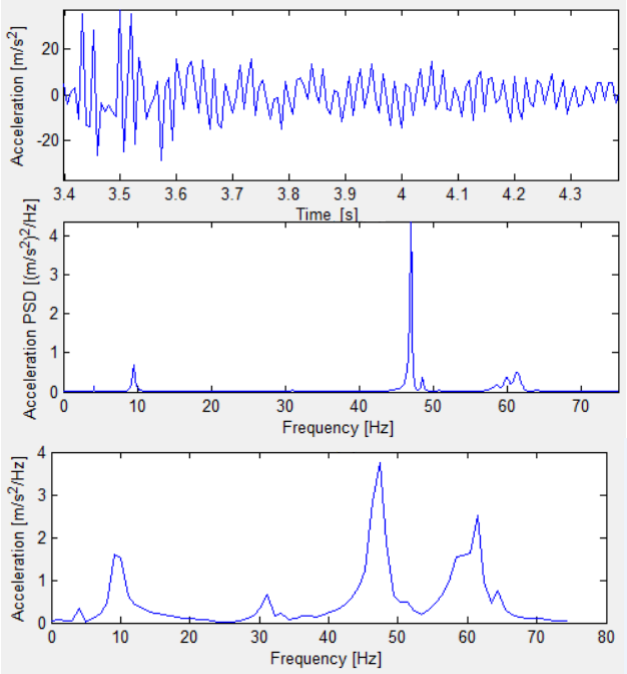

Fig. 8 Setup 1, pre-stress level 4, signal 4x: (from top to bottom) square acceleration in time domain, power spectral density (PSD) of the acceleration and the acceleration in frequency domain

Figure 9 shows the additional PSD diagrams of the signals 4y and 4z for the setup 1 and the pre-stress level 1. These signals are extracted from the direction Y and Z of the accelerometer in the node 4.

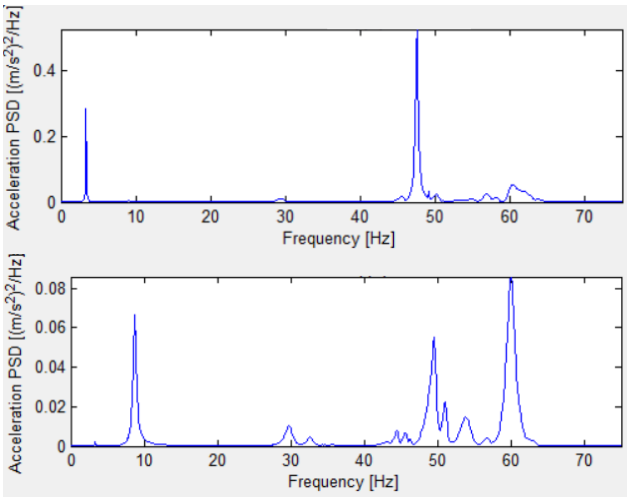

Fig. 9 Setup 1, pre-stress level 1, power spectral density (PSD) of signal 4y (top) and 4z (bottom)

Analysis of all three PSD signals 4x (Fig. 7), 4y and 4z (Fig. 9) shows that some of the natural frequencies and corresponding modes are more or less visible depending on the direction of the measured signal. The more natural frequencies and modes are induced, the better estimation of the modal parameters can be done. The modal parameters shown here in Tab. 9 are obtained based on the combining modal information from the nine different setups into one single mode.

3.5. Eigenmodes and eigenfrequencies

The first five identified natural frequencies and damping ratios for the pre-stress level 1 and 4 are shown in Tab. 9, while first five eigenmodes for the pre-stress level 4 are presented in Figs. 10 – 14. The first identified mode is a rotation of the upper triangle along the vertical axis of the simplex.

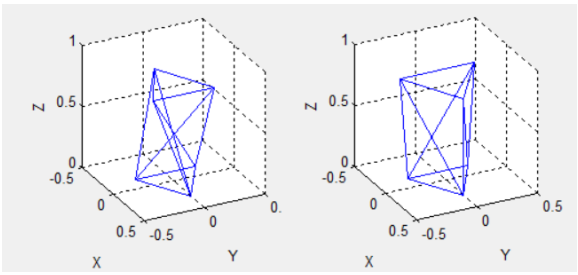

Fig. 10 Pre-stress level 4, mode 1 (4.12 Hz). Rotation of the upper triangle along the Z axis

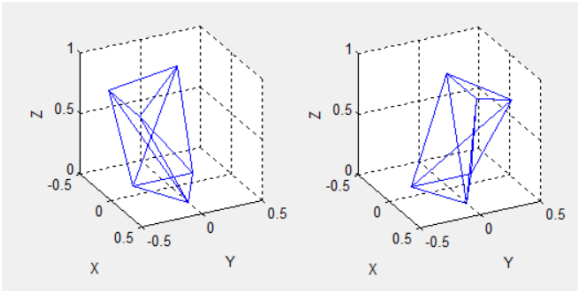

Fig. 11 Pre-stress level 4, mode 2 (9.67 Hz). Rotation of the upper triangle along the Y axis

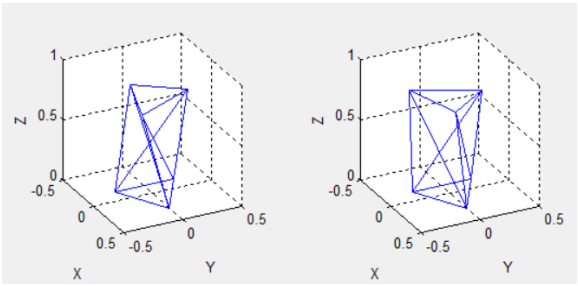

Fig. 12 Pre-stress level 4, mode 3 (30.85 Hz). Nodes of the upper triangle change distance between themselves with additional rotation along the Y axis

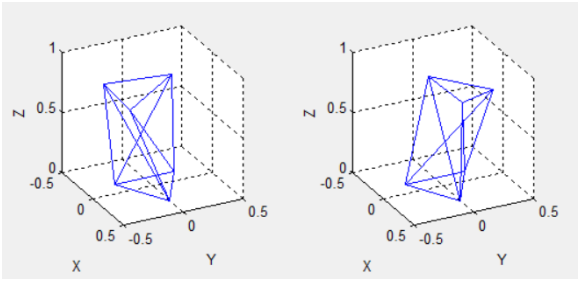

Fig. 13 Pre-stress level 4, mode 4 (47.14 Hz). Rotation of the upper triangle along the Y axis

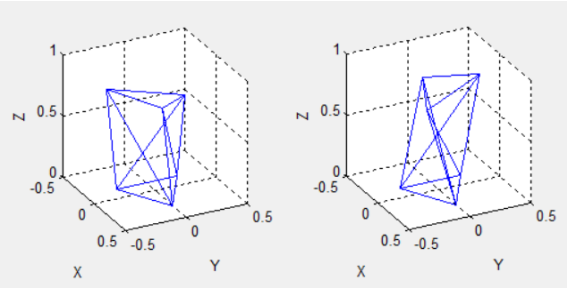

Fig. 14 Pre-stress level 4, mode 5 (60.04 Hz). Nodes of the upper triangle change distance between themselves with additional rotation along the Y axis

The resonance spectrum of a tensegrity structure often includes very closely situated frequencies, which are resulting from a high degree of symmetry or repetitivity in the structure. Coinciding natural frequencies are an obstacle in measuring and analyzing the correct resonance. In this experiment third, fourth and fifth frequencies presented in Tab. 9 had a very closely related double eigenmode. Hence, the results of these frequencies were at some point a matter of arbitrary selection. On the other hand, it would be advantageous if the lowest natural frequency of the structure could be easily measured and filtered from the whole spectrum. In these tests, the first two natural frequencies were easily recognizable, which for the vibrational health monitoring purposes is commonly utilized and sufficient.

4. SUMMARY AND CONCLUSIONS

The susceptibility of tensegrity structures to vibrations can be a prime design issue in their mechanics. It is also of growing importance because of the their slenderness and also of their dynamic loading. The experimental verification of design values, in particular modal parameters (eigenfrequencies, damping ratios, mode shapes, and modal scaling factors), can be essential for design and model validation of the tensegrity structure and for guaranteeing the their safety and serviceability. It can be also employed for quality control and structural health monitoring purposes.

In the paper it was shown that the modal parameters of the simplex tensegrity prism may be determined experimentally in the form of the eigenfrequencies, eigenmodes and damping ratios. They can be also obtained via the finite element method and own program which is currently implemented by the authors. However, although the natural frequencies in tensegrity structures are important in the vibrational health monitoring, it is not always possible to use them as an indicator of the pre-stress level and hence as the indicator of the structure stiffness. In numerical simulations, the stiffness can be easy regulated and improved by changing the level of pre-stress. In practice, however, there are some difficulties and an experimental validation can be advantageous, especially if the natural frequencies of the structure are measured and filtered from the whole experimental vibration spectrum.

The mechanical response of such structures can be complicated, in particular the dynamic response and behaviour in the self-stress states, which require a precise physical model enabling to estimate the pre-stress values (experimental tests) and a more complex numerical models due to the determinant of the A matrix equal to zero and the necessity of building the additional tangent stiffness matrix.

Another important conclusion is the fact, that an analysis of only one second of the acceleration in the time domain leads to a very rich portion of information. The data could be gathered in real time for the purposes of structural health monitoring.

REFERENCES

1. R. Motro: Tensegrity: structural systems for the future. UK 2003.
2. R.E. Skelton, M. C. de Oliveira: Tensegrity systems. London 2009.
3. F. Fraternali, G. Carpentieri, A. Amendola: On the mechanical modeling of the extreme softening/stiffening response of axially loaded tensegrity prisms. Journal of the Mechanics and Physics of Solids, 74, 2015, pp.136-157.
4. A. Amendola, G. Carpentieri, M. de Oliveira, R.E. Skelton, F. Fraternali: Experimental investigation of the softening-stiffening response of a tensegrity prisms under compressive loading. Composite Structures, 117, 2014, pp.234-243.
5. L. Małyszko: Static response of axially loaded tensegrity prism. Example of using proprietary programming language. In L. Małyszko & R. Tarczewski (Eds.), Lightweight Structures in Civil Engineering - LSCE 2016. Contemporary Problems. University Publishing House, Olsztyn 2016, pp. 43–48.
6. L. Małyszko: Design of tensegrity modules with UHMWPE cables based on experiments and nonlinear behaviour. In J.Obrębski (Ed.), Lightweight Structures in Civil Engineering – LSCE 2017. Contemporary Problems. Bydgoszcz 2017.
7. R. Motro, S.Najari, P. Jouanna: Static and dynamic analysis of tensegrity systems. In G. De Rock et al. (Eds.), Shell and Spatial Structures: Computational Aspects, Springer-Verlag Berlin, 1987.
8. N. Ashwear, A. Eriksson: Natural frequencies describe the pre-stress in tensegrity structures. Computers and Structures, 138, 2014, pp. 162-171.
9. S. Amouri, J. Averseng, J. Quirant, J.F. Dube: Structural design and control of modular tensegrity structures. European journal of Environmental and Civil Engineering, 19:6, 2016, pp. 687-702.
10. R. Motro: Tensarch Project. In T. Telford (Eds.), First international conference on space structures, Guilford (UK), 2002, pp. 57-66.
11. N. Bel Hadj Ali, I.F.C. Smith: Dynamic behavior and vibration control of a tensegrity structure. International Journal of Solids and Structures, 47, 2010, pp. 1285-1296.
12. A. Kasprzak: Ocena możliwości wykorzystania konstrukcji tensegrity w budownictwie mostowym. PhD thesis under supervision of W. Gilewski, Warsaw University of Technology, 2014.
13. E. Reynders, M. Schevenels, G. de Roeck: MACEC 3.3. A Matlab toolbox for experimental and operational modal analysis. User Manual, Leuven, 2014.
14. MATLAB2014a. Programming language of The MathWorks, Inc. http://www.mathworks.com/
15. B. Peeters, H. Van der Auweraer, P. Guillaume, J. Leuridan: The PolyMax frequency-domain method: a new standard for modal parameter estimation? Shock and Wibration 11, 2004, pp.395-409.
16. P. Guillaume, P. Verboven, S. Vanlanduit, H. Van der Auweraer, B. Peeters: A poly-reference implementation of the least-squares complex frequency domain-estimator. In: Proceedings of the 21st international modal analysis conference, Kissimmee, Florida, USA.